Output Amplifier Phase Compensation for Improved Filter Performance of Feedforward Active EMI Filters

M.Sc. Stefan Haensel, Siemens AG, Germany
M.Sc. Thomas Polster, Siemens AG, Germany
Prof. Dr.-Ing. Stephan Frei, TU Dortmund, Germany

1 Introduction

In power electronic systems EMI is generated by the switched operation of semiconductor devices. To comply with given EMC standards often filters need to be integrated into the system. Since filters are bulky and heavy, active filters were proposed by [1–3]. **A**ctive **E**MI **F**ilters (AEF) are active components, which inject an anti-EMI signal into the system to cancel out the EMI. AEFs can be implemented as feedforward and feedback topologies [4]. Feedforward AEF measure from the source injected EMI and generate an anti-EMI signal. They need a very precise design of the circuit to achieve a good attenuation but are stable without any measures. Therefore a better attenuation is expected from feedforward topologies [5, 6]. In previous publications many components of a **f**eed**f**orward **c**urrent **s**ense **c**urrent **i**njection (FF CSCI) topology were already optimized, compare e.g. [6]. However most publications focus on low-power applications, where no additional power amplifier is needed to reach a sufficiently high anti-EMI level, e.g. [7]. However, the amplifier is a significant limitation for the performance of an FF high-power AEF. The contribution of this paper is a phase compensation strategy for high-power analog amplifiers, which improves the high-frequency attenuation of a FF AEF by more than 40 dB compared to [8].

2 Introduction of the target application

As a target application a three-phase grid-connected AC/DC converter is assumed. The overall structure is shown in Figure 3. It consists of three voltage sources, representing the grid voltage, a grid inductance L_{grid}, a line impedance stabilization network (LISN), a filter, a converter with a DC link capacitor C_{DC} and a load. The filter comprises a common mode (CM) choke L_{CM}, x-capacitors C_{x}, an y-capacitor C_{y} and a differential mode (DM) choke L_{DM}. All parasitic capacitance of the setup against ground can be summarized in C_{par}. In this contribution an AEF shall be used to improve the CM attenuation of the filter without increasing the leakage current. For an analytical investigation of the CM behavior of the system, it will be transferred to its CM equivalent circuit [9] and then simplified. The LISN decouples the system from the grid. Its impedance can be

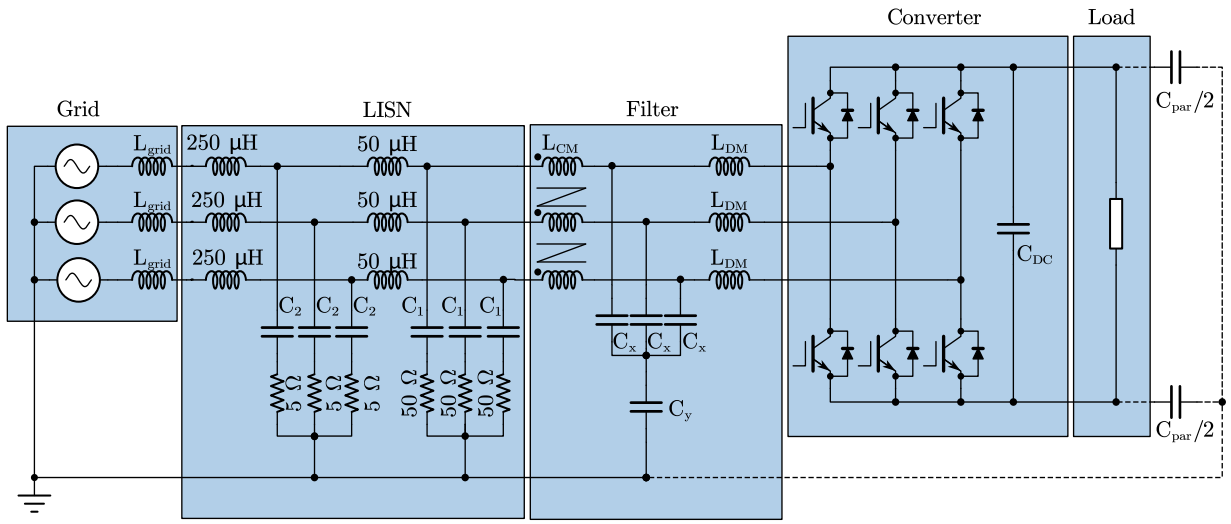

Figure 1: Diagram of a three-phase AC/DC converter system with LISN and filter

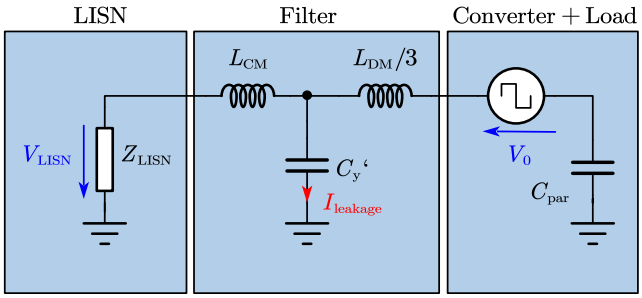

Figure 2: Simplified CM equivalent circuit of the three-phase AC/DC converter system

summarized to Z_{LISN}. The converter can be represented by a voltage source V_0, which is connected between the parasitic capacitance C_{par} and the filter. The simplified CM equivalent circuit is shown in Figure 2.

A FF CSCC AEF can be used to compensate for the voltage drop across the y-capacitor [7], which virtually increases the capacitance of the y-capacitor. To achieve this, a current transformer (G_{CT}) measures the CM current of the converter. A high-pass filter (G_{HP}) attenuates low frequency harmonics, which have high power, to protect the AEF against saturation and reduce losses. An integrator (G_{Int}) models the impedance of the y-capacitor and an inverting amplifier (G_{Inv}) amplifies and inverts the signal for high power compensation. The structure of the FF CSCC AEF is shown

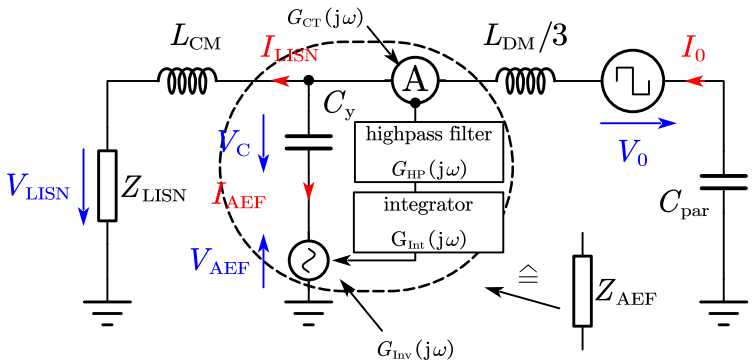

Figure 3: General structure of a feedforward current sense current compensating active EMI filter

in Figure 3.

The AEF voltage V_{AEF} can be expressed by the cascaded transfer functions of the current transformer, the high-pass filter, the integrator, and the inverting amplifier:

$$V_{\mathrm{AEF}} = G_{\mathrm{Inv}} \cdot G_{\mathrm{Int}} \cdot G_{\mathrm{HP}} \cdot G_{\mathrm{CT}} \cdot I_0 \tag{1}$$

The AEF can be seen as an impedance Z_{AEF}, which can be expressed by the y-capacitors voltage V_{C}, the AEF voltage and the current through the branch I_{AEF}.

$$Z_{\mathrm{AEF}} = \frac{V_{\mathrm{C}} - V_{\mathrm{AEF}}}{I_{\mathrm{AEF}}} \tag{2}$$

The current can be expressed by the capacitor voltage V_{C} and its impedance Z_{Cy}.

$$I_{\mathrm{AEF}} = \frac{V_{\mathrm{C}}}{Z_{\mathrm{Cy}}} \tag{3}$$

$$Z_{\mathrm{Cy}} = \frac{1}{j\omega C_{\mathrm{y}}} \tag{4}$$

By using the equation for a current divider, the current through this branch can be expressed by the CM current of the converter I_0. Since the impedance of the LISN and the CM choke is much larger than the impedance of the AEF, I_{AEF} can be approximated to be I_0.

$$I_{\mathrm{AEF}} = \frac{Z_{\mathrm{LISN}} + \mathrm{j}\omega L_{\mathrm{CM}}}{Z_{\mathrm{AEF}} + Z_{\mathrm{LISN}} + \mathrm{j}\omega L_{\mathrm{CM}}} I_0 \approx I_0 \qquad (5)$$

$$|Z_{\mathrm{LISN}} + j\omega L_{\mathrm{CM}}| \gg Z_{\mathrm{AEF}}$$

A current ratio G_{I} can be introduced, which describes the relation between the current flowing through the LISN and the current flowing through the AEF.

$$G_{\mathrm{I}} = \frac{I_{\mathrm{LISN}}}{I_{\mathrm{AEF}}} = \frac{Z_{\mathrm{AEF}}}{Z_{\mathrm{LISN}} + j\omega L_{\mathrm{CM}}} \qquad (6)$$

$$\begin{aligned} G_{\mathrm{I}} &= \frac{V_{\mathrm{C}} - I_0 \cdot G_{\mathrm{Int}} \cdot G_{\mathrm{HP}} \cdot G_{\mathrm{CT}}}{I_{\mathrm{AEF}} \cdot (Z_{\mathrm{LISN}} + \mathrm{j}\omega L_{\mathrm{CM}})} \\ &\approx \frac{V_{\mathrm{C}} - \frac{V_{\mathrm{C}}}{Z_{\mathrm{Cy}}} \cdot G_{\mathrm{Int}} \cdot G_{\mathrm{HP}} \cdot G_{\mathrm{CT}}}{I_{\mathrm{AEF}} \cdot (Z_{\mathrm{LISN}} + \mathrm{j}\omega L_{\mathrm{CM}})} \\ &= \frac{Z_{\mathrm{Cy}}}{(Z_{\mathrm{LISN}} + \mathrm{j}\omega L_{\mathrm{CM}})} \cdot \left(1 - G_{\mathrm{Inv}} \cdot \frac{G_{\mathrm{Int}}}{Z_{\mathrm{C}}} \cdot G_{\mathrm{HP}} \cdot G_{\mathrm{CT}}\right). \end{aligned} \qquad (7)$$

The insertion loss (IL) can be defined as the current ratio G_{I} if the AEF is active divided by the current ratio $G_{\mathrm{I}}|_{V_{\mathrm{AEF}}=0}$ if the AEF is deactivated and its output voltage is zero.

$$\begin{aligned} IL_{dB} &= 20\log_{10}\left(\frac{|G_{\mathrm{I}}|}{|G_{\mathrm{I}}|_{V_{\mathrm{AEF}}=0}}\right) \\ &= 20\log_{10}\left(\left|1 - G_{\mathrm{Inv}} \cdot \frac{G_{\mathrm{Int}}}{Z_{\mathrm{Cy}}} \cdot G_{\mathrm{HP}} \cdot G_{\mathrm{CT}}\right|\right) \end{aligned} \qquad (8)$$

3 Analytical optimization of the output amplifier

In this contribution, only the impact of the inverting amplifier and its impact on the IL will be analyzed. Therefore G_{HP} and $\frac{G_{\mathrm{Int}}}{Z_{\mathrm{Cy}}}$ will be assumed to be one. G_{CT} will be assumed to be minus one. Then the IL only depends on $1 + G_{\mathrm{Inv}}$. An overview of the achievable IL based on the amplitude and phase of the transfer function of the inverting amplifier can be found in Figure 4.

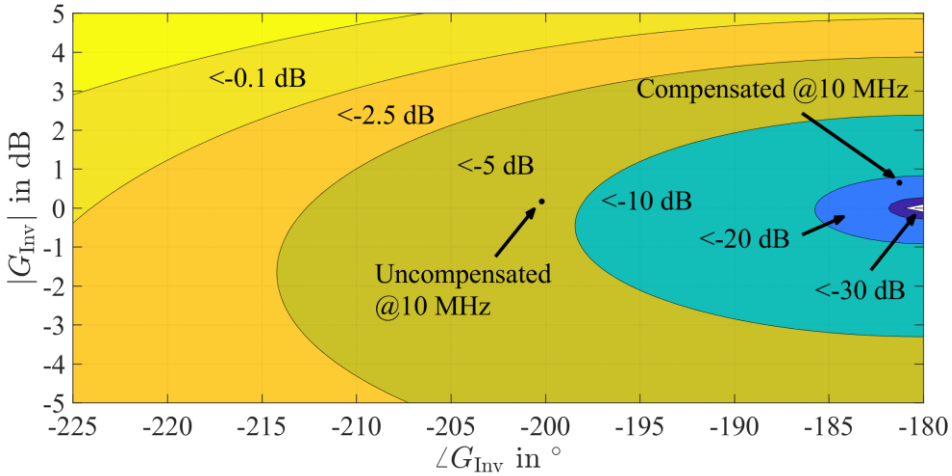

Figure 4: IL_{dB} in dependency of amplitude a phase of the transfer function of the inverting amplifier

It can be seen, that, e.g., only more than 20 dB IL can be reached, if the amplitude stays between ± 0.9 dB and the phase stays above -186°.
The output amplifier can be either implemented based on discrete devices or with a high-power operational amplifier. In this contribution, the focus is on an implementation with an operational

amplifier. One example of such an amplifier is the current feedback amplifier ADA4870 from Analog Devices [10]. The open loop transimpedance can be expressed by a transfer function with a denominator of fourth order with one pole at 14 kHz and three poles at 130 MHz. The close loop response for a current feedback amplifier in inverse configuration is given by (9) [11].

$$G_{\mathrm{Inv}} = -\frac{Z_{\mathrm{ol}} \cdot R_{\mathrm{fb}}}{Z_{\mathrm{in}}(Z_{\mathrm{ol}} + R_{\mathrm{fb}})} \tag{9}$$

R_{fb} represents the feedback resistor and Z_{in} the impedance at the input of the amplifier. For a purely resistive impedance at the input of $1200\ \Omega$ and a feedback resistor of $1200\ \Omega$, the frequency response is shown in Figure 6 as “uncompensated”. The close loop response has a very good amplitude response, which is close to 0 dB up to 30 Mhz. But the phase starts already to decrease

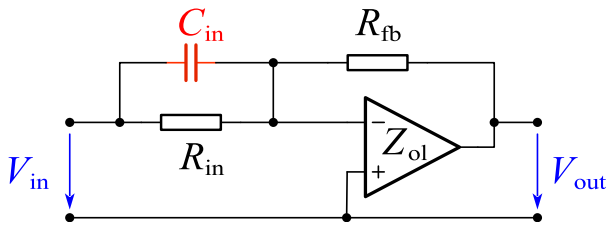

Figure 5: Inverting amplifier with phase compensating capacitor C_{in}

from 1 MHz. At 10 MHz the amplitude is slightly increased to 0.17 dB and the phase reached 200.2°. This point is added to Figure 4 as “uncompensated @10 Mhz”. It can be seen, that this phase shift limits the IL to 9 dB. To improve the amplifier behavior a phase compensation can be implemented. A phase compensation can be realized by the introduction of an additional zero in G_{Inv} by introducing a pole in Z_{in}, which can be built up by a parallel connection of an input resistor R_{in} and input capacitor C_{in}. The corresponding schematic is shown in Figure 5.
Since only the feedback resistor R_{fb} defines the stability of a current feedback amplifier, there are no limitations for the input capacitor C_{in}. The close loop response for an input capacitance of $4.5\ \mathrm{pF}$ is shown in Figure 6 as “compensated”. It can be seen, that the phase stays at 180° up to 6 MHz. At 10 MHz the amplitude of the compensated amplifier is increased to 0.65 dB, but its phase decreased to -181.3° only. The achievable IL at 10 MHz can be therefore calculated to -21 dB. The corresponding point is labeled as “Compensated @10 MHz” in Figure 4.

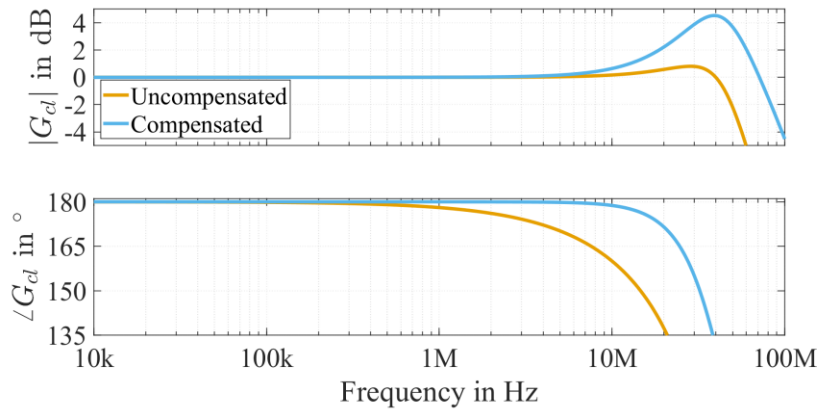

Figure 6: Close loop frequency response in inverse amplifier configuration with and w/o compensation

4 Validation in a laboratory setup

To validate the results a printed circuit board (PCB) was designed and populated. It is shown in Figure 7. It holds the high-pass filter, the integrator, the inverting amplifier, and a CM equivalent circuit based on Figure 3. For validation, the transfer function of the circuit was measured with a

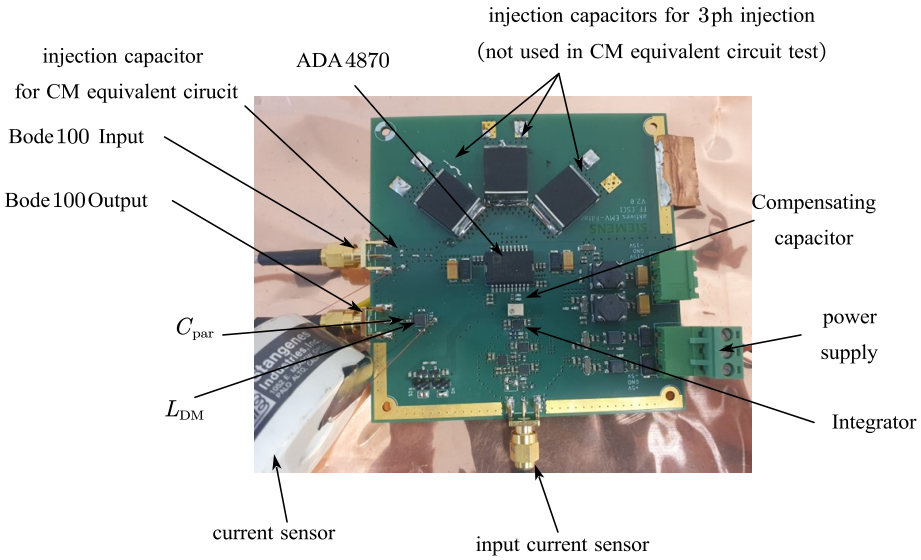

Figure 7: Printed circuit board with high-pass filter, integrator, inverting amplifier and CM equivalent circuit

vector network analyzer (Bode 100 from Omicron) The measurement results are shown in Figure 8. It can be seen, that at 50 kHz an attenuation of more than 44 dB can be achieved with the AEF. But without compensation, the attenuation decreases significantly starting from 100 kHz. With attenuation an additional 26.4 dB can be achieved at 356 kHz. This points out the effectiveness of the phase compensation of the inverting amplifier.

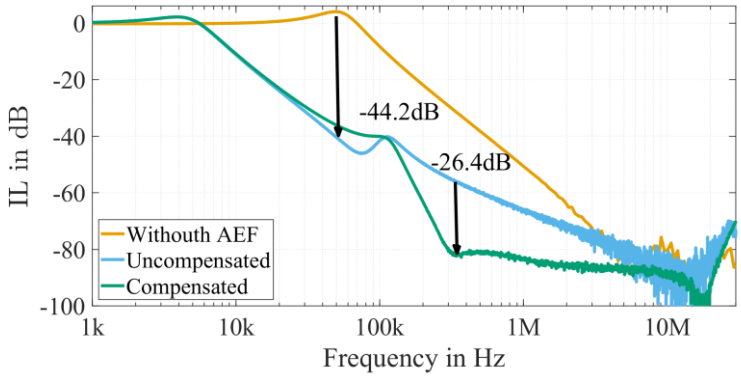

Figure 8: Measurement results of the vector network analyzer Bode 100 at the CM equivalent circuit

In a second setup, a bidirectional 16 kW three-phase AC/DC converter was equipped with the FF CSCC AEF. The setup is shown in Figure 9. Three measurements were conducted with a Rohde&Schwarz EMI test receiver ESR7. First, a measurement, where the AEF was disabled (“AEF off”). In a second measurement, the AEF was switched on, but without the compensating capacitor populated (“With uncompensated AEF”). In a third measurement, a compensation capacitor of $4.5\,\mathrm{pF}$ was used. The measurement results are shown in Figure 10. A good attenuation of the AEF can be noticed up to frequencies of 150 kHz even without compensation. However, at higher frequencies the compensation improves the attenuation of the AEF. At 360 kHz an improvement of 21 dB can be observed.

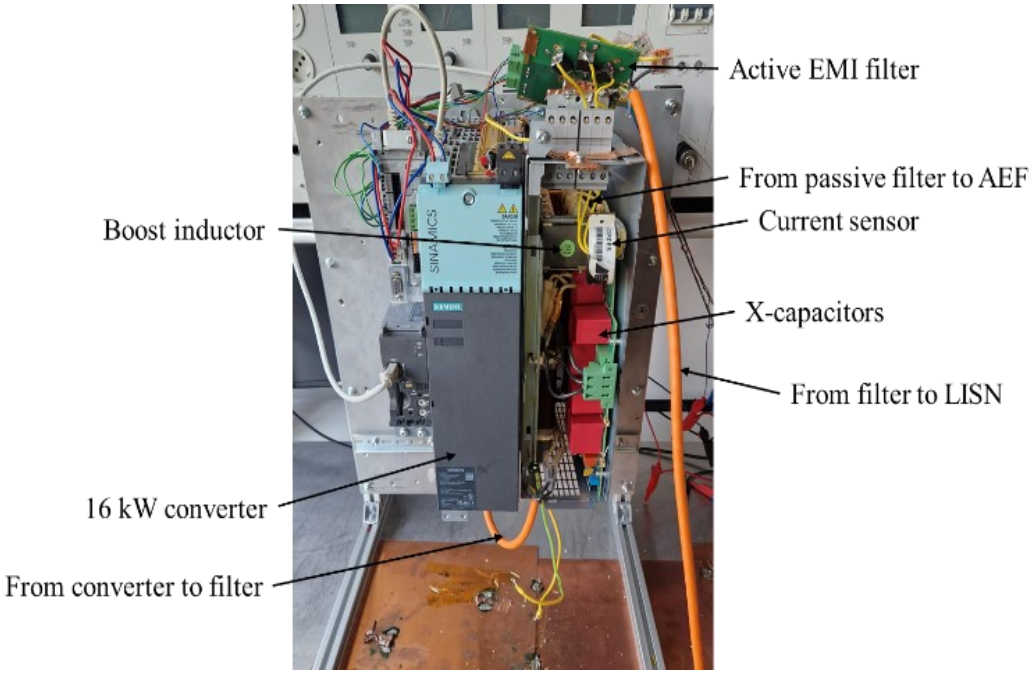

Figure 9: Laboratory setup with a bidirectional 16 kW three-phase AC/DC converter equipped with FF CSCC AEF

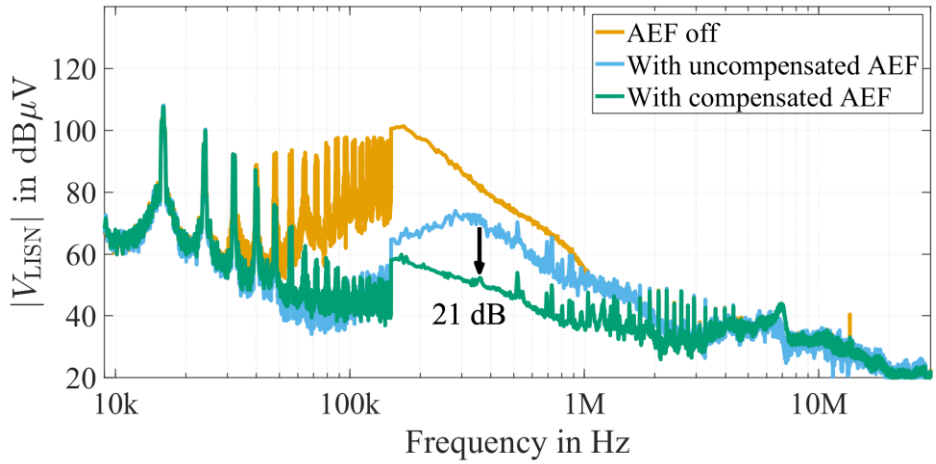

Figure 10: EMI measurement results for the 16 kW AC/DC converter without AEF, with uncompensated AEF and with compensated AEF

5 Conclusion

This contribution shows the limitation of the insertion loss (IL) of a feedforward active EMI filter due to the frequency characteristic of the inverting output amplifier. Due to the phase lag of the used amplifier the IL is limited to 9 dB at 10 MHz. The transfer function of the amplifier can be improved by a phase compensation, which only needs one capacitor with a very small value in the range of pico Farads, with a price of a few cents. With this compensation the IL can be improved by more than 40 dB in theory and by 21 dB in a laboratory setup with a 16 kW AC/DC converter, which makes the feedforward approach competitive to feedback approaches.

Literatur

[1] S. Feng, W. Sander und T. Wilson, "Small-capacitance nondissipative ripple filters for DC supplies", *IEEE Trans. Magn.*, Jg. 6, Nr. 1, S. 137–142, 1970, doi: 10.1109/TMAG.1970.1066675.

[2] L. LaWhite und M. F. Schlecht, "Design of active ripple filters for power circuits operating in the 1-10 MHz range", *IEEE Trans. Power Electron.*, Jg. 3, Nr. 3, S. 310–317, 1988, doi: 10.1109/63.17949.

[3] L. E. LaWhite und M. F. Schlecht, "Active filters for 1 MHz power circuits with strict input/output ripple requirements" in *1986 17th Annual IEEE Power Electronics Specialists Conference*, Vancouver, Canada, 1986, S. 255–263, doi: 10.1109/PESC.1986.7415569.

[4] Y.-C. Son und S.-K. Sul, "Generalization of active filters for EMI reduction and harmonics compensation", *IEEE Trans. on Ind. Applicat.*, Jg. 42, Nr. 2, S. 545–551, 2006, doi: 10.1109/TIA.2006.870030.

[5] D. Shin, S. Jeong, Y. Baek, C. Park, G. Park und J. Kim, "A Balanced Feedforward Current-Sense Current-Compensation Active EMI Filter for Common-Mode Noise Reduction", *IEEE Trans. Electromagn. Compat.*, Jg. 62, Nr. 2, S. 386–397, 2020, doi: 10.1109/TEMC.2019.2906854.

[6] S. Jeong, J. Park und J. Kim, "A Customized Integrated Circuit for Active EMI Filter With High Reliability and Scalability", *IEEE Trans. Power Electron.*, Jg. 36, Nr. 11, S. 12631–12645, 2021, doi: 10.1109/TPEL.2021.3083286.

[7] Z. Zhang und A. M. Bazzi, "A Virtual Impedance Enhancement Based Transformer-Less Active EMI Filter for Conducted EMI Suppression in Power Converters", *IEEE Trans. Power Electron.*, Jg. 37, Nr. 10, S. 11962–11973, 2022, doi: 10.1109/TPEL.2022.3172388.

[8] Stefan Haensel und Stephan Frei, "Gain Adjustment Control for an Active EMI Filter" in *PCIM Europe 2023*, S. 2435–2441, doi: 10.30420/566091335.

[9] A. D. Brovont und S. D. Pekarek, "Derivation and Application of Equivalent Circuits to Model Common-Mode Current in Microgrids", *IEEE J. Emerg. Sel. Topics Power Electron.*, Jg. 5, Nr. 1, S. 297–308, 2017, doi: 10.1109/JESTPE.2016.2642835.

[10] Analog Devices, "ADA4870 High Speed, High Voltage, 1 A Output Drive Amplifier" [Online]. Verfügbar unter: https://www.analog.com/media/en/technical-documentation/data-sheets/ADA4870.pdf

[11] L. v. Wangenheim, *Analoge Signalverarbeitung: Systemtheorie, Elektronik, Filter, Oszillatoren, Simulationstechnik*. Wiesbaden: Vieweg+Teubner, 2010.